



# COMPUTATIONAL SIMULATION OF DISCONTINUOUS FAILURE PROCESSES

K. Willam and M.-M. Iordache

Department of Civil, Environmental, and Architectural Engineering,  
University of Colorado, Boulder, CO 80309-0428, USA

## **Summary:**

Our contribution examines discontinuous failure processes in quasi-static environments. To this end, we first discuss the loss of continuity in solids at the local level of materials, and subsequently at the global level of structural systems. These local and global failure indicators are formalized in terms of localization conditions that are illustrated with the aid of transformed Mohr stress coordinates.

For definiteness, the discontinuous failure process is illustrated with the example problem of a Drucker-Prager material that is used to describe the matrix behavior of a two-phase particle composite. For illustration, progressive failure in a representative composite specimen is evaluated with regard to the respective energy absorption capacity in uniaxial compression.

## **Resumen:**

La ponencia examina los procesos de fallo o rotura con discontinuidad en un entorno cuasi-estático. Para ello, se discute primero la pérdida de continuidad en sólidos a nivel local del material, y seguidamente al nivel global de sistemas estructurales. Los indicadores de rotura locales y globales se formalizan en términos de las condiciones de localización y de argumentos de Mohr.

El proceso de rotura o fallo con discontinuidad se ilustra mediante el ejemplo de una probeta de material tipo Drucker-Prager sometida a compresión. La misma formulación de material elastoplástica se utiliza también para describir el comportamiento de la matriz en un material compuesto de partículas. La rotura progresiva en las probetas de material uniforme y de material compuesto se comparan y se evalúan en relación a sus respectivas capacidades de absorción de energía.

## **INTRODUCTORY REMARKS**

Deterioration science, and in particular the evaluation of degradation processes, are recent initiatives by the Engineering Division of the US-National Science Foundation with the aim to enhance the current state of Civil Infrastructure Systems. At the core of this effort stands the behavior of engineering materials and the description of the constitutive behavior to predict load capacity and life expectancy of ageing and deteriorating structures. In the case of cohesive-frictional materials, such as concrete and geomaterials, a realistic constitutive description depends critically on the treatment of the low cohesive strength and its ability to capture tensile cracking. In addition, it has to properly account for the pressure-sensitivity of internal friction and the concomitant loss of normality (loss of symmetry). Consequently, degradation analysis of cohesive-frictional materials is a pressing issue,

not only when severe overloads are considered, e.g. due to earthquake and impact loading, but also when gradual deterioration under service load conditions is to be evaluated due to hygrothermal ageing and environmentally induced damage.

Recent advances of computational methods, and the finite element analysis in particular, have made it possible to evaluate the nonlinear and inelastic performance of complex structural components in three dimensions. Thereby, the material behavior is at the center of such assessments that require numerical integration of nonlinear tensor-valued rate (differential) equations. Consequently, the incremental tracing of the response history and the proper treatment of singular points are critical when failure initiation at the material level and failure propagation at the structural level are to be captured. In short, there is an urgent need for quantitative analytical solutions to assess the local state of material deterioration and for the efficient and robust computational treatment that captures the progressive failure process at the structural level without undue bias.

### DISCONTINUOUS FAILURE AT THE MATERIAL LEVEL

Clearly failure is a non-local and dynamical process when local material defects propagate through the solution domain subjected to non-uniform conditions. Consequently we are facing the solution of initial boundary value problems, in which local material failure initiates the progressive failure process within the structure, that might evolve in a ductile or brittle manner depending on the confinement level.

In order to rationalize failure initiation and failure propagation, we need first to discuss the manifestation of degradation processes that take place at the material level. To this end we define failure as a process in which the continuity relations of classical continua are relaxed, and in which jumps in the field variables appear due to loss of regularity, see [1], and [2].

- In ductile failure, the displacement (velocity) field remains continuous at the macroscopic level as well as their time/space derivatives - we speak of diffuse (distributed) failure when the kinematic compatibility conditions are satisfied fully.
- In localized failure certain components of the strain tensor and the stress tensor exhibit jump conditions. This is traditionally the realm of localization analysis of weak discontinuities, where the material remains competent, i.e. the contiguity of neighboring particles is fully maintained, but discontinuities arise in the higher derivatives of space and/or time.
- In brittle failure, the tangential displacement (velocity) components, and in the case of tensile cracking also the normal displacement (velocity) components, exhibit jumps across a discontinuity surface. This is traditionally the realm of discrete fracture analysis of strong discontinuities when contact and decohesive interface behavior determines the degradation of surface tractions.

The formation of Lüders bands coincides with the onset of localized deformations, when the stress level reaches a critical value during yielding [3] and [4]. Thus shear band formation is the result. Localization may be viewed as a bifurcation phenomenon that can be predicted in terms of pre-localized constitutive properties of the material. If the material is rate-independent, then critical conditions appear when the constitutive relations allow for bifurcation from a homogeneous or smoothly varying deformation field into a field, in which first weak, and subsequently strong discontinuities appear. This bifurcation condition coincides with the stationarity condition of acceleration (stress) waves, i.e. localization analysis may be considered as a search for stationary acceleration waves (standing waves).

We say that there exists a *discontinuity of order  $n$*  in a continuum, if any of the  $n$ -th partial space or time derivatives of the field exhibits a jump across the surface  $\mathcal{S}$  (figure 1, left). Let  $\mathcal{S} \subset \mathcal{D}$  be a surface that separates the domain in two parts,  $\mathcal{D}^+$  and  $\mathcal{D}^-$  ( $\mathcal{D}^+ \cup \mathcal{D}^- = \mathcal{D}$ ,  $\mathcal{D}^+ \cap \mathcal{D}^- = \emptyset$ ), then the jump of the function  $\phi : \mathcal{D} \rightarrow \mathbb{R}^3$  across the surface  $\mathcal{S}$  is defined as  $[\phi] = \phi^+ - \phi^-$ . We

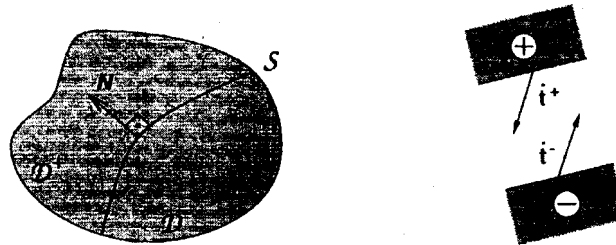


Figure 1: *Discontinuity Surface Exhibiting Traction Continuity.*

speak of weak and strong discontinuities depending on the severity of jumps in the kinematic fields.

**Hadamard's Compatibility Condition:** The general theory of the acceleration waves was originally formulated in [5]. According to Hadamard, waves are:

“An isolated geometric surface (not necessarily plane) that moves relatively to the material, across which certain field variables are momentarily discontinuous.”

An acceleration wave implies the existence of second order discontinuities in the displacement field, while the first order derivatives are still continuous ( $\mathbf{u}(\mathbf{x}, t) \in C^1$ ). Consequently, we speak of formation of weak discontinuities.

Let  $S$  be a discontinuity surface of 1-st order for  $\phi(\mathbf{x}, t)$  (see figure 1). Then the function is continuous  $\phi \in C^0$  and does not exhibit jumps along the discontinuity surface,  $[d\phi] = 0$  [6]. If  $c$  denotes the propagation speed and  $N$  the propagation direction of the wave front, then the following expressions must hold:

$$\mathbf{x} = \mathbf{x}_0 + N c t \quad \frac{\partial \mathbf{x}}{\partial t} = N c \quad (1)$$

$$0 = [d\phi] = \left[ \frac{\partial \phi}{\partial \mathbf{x}} \frac{\partial \mathbf{x}}{\partial t} dt + \frac{\partial \phi}{\partial t} dt \right] = [\phi_{,i} N_i c dt + \dot{\phi} dt] \quad (2)$$

$$\Leftrightarrow c [\phi_{,i}] N_i = -[\dot{\phi}] \quad (3)$$

As  $\nabla_{\mathbf{x}} \phi$  can only exhibit jumps along the propagation direction  $N$ , we can write  $[\phi_{,i}] = \alpha N_i$ . This results in the general Hadamard's compatibility condition that interrelates time and space derivatives along the discontinuity surface,

$$c [\phi_{,i}] = -[\dot{\phi}] N_i \quad (4)$$

This equality has to be satisfied by any  $C^0$  continuous field in the domain  $\mathcal{D}$ . It states that jumps of the spatial derivatives may only occur normal to the discontinuity surface, and that the jumps of the space and time derivatives are negative proportional to the propagation velocity.

**Remark:** Recall that displacement-based finite element formulations maintain interelement continuity for conforming element formulations, but they exhibit jumps of the normal derivatives along the element interfaces. This relaxation of kinematic regularity arises as the weak equilibrium statement of the virtual work principle relaxes the minimum continuity requirements of the displacement field from  $\mathbf{u}(\mathbf{x}, t) \in C^1$  down to  $\mathbf{u}(\mathbf{x}, t) \in C^0$ .

### **Stationary Condition of Elastoplastic Body Waves**

At the outset we mentioned that the localization condition corresponds to the formation of stationary

acceleration waves. In order to examine the appearance of standing body waves in elastoplastic solids we need to consider the rate form of equilibrium and the consequences of second order discontinuities in the displacement field  $\mathbf{u}(\mathbf{x}, t) \in C^1$ , with spatial and time derivatives that are  $C^0$  continuous,

$$\epsilon = \frac{1}{2} (\nabla_x^t \mathbf{u} + \nabla_x \mathbf{u}) \in C^0 \quad \text{and} \quad \mathbf{v} = \frac{\partial \mathbf{u}}{\partial t} \in C^0 \quad (5)$$

If the material is elastic on both sides of the discontinuity surface  $\mathcal{S}$ , and the same elasticity tensor relates stresses to strains ( $\mathbf{E}_s^+ = \mathbf{E}_s^- = \mathbf{E}_s$ ), then the stress tensor is also  $\boldsymbol{\sigma}(\mathbf{x}, t) \in C^0$  continuous. The Hadamard compatibility condition (4) requires that the velocity and stress fields satisfy :

$$c [v_{i,j}] = -[\dot{v}_i] N_j \quad (\forall) i, j \in \{1, 2, 3\} \quad (6)$$

$$c [\sigma_{ij,k}] = -[\dot{\sigma}_{ij}] N_k \quad (\forall) i, j, k \in \{1, 2, 3\} \quad (7)$$

Letting  $k \rightarrow i$  in (7), the equation of motion,  $\sigma_{ij,i} = \rho \dot{v}_j$ , in the absence of the body forces transforms into

$$-[\dot{\sigma}_{ij}] N_i = \rho c [\dot{v}_j] \quad (8)$$

Introducing the elastic constitutive law, the strain-displacement relations, and taking advantage of the minor symmetry in  $E_{ijkl}^o = E_{ijlk}^o$

$$\rho c^2 [\dot{v}_j] = -c N_i E_{ijkl}^o [\dot{\epsilon}_{kl}] = -\frac{1}{2} c N_i E_{ijkl}^o ([v_{i,k}] + [v_{k,i}]) = N_i E_{ijkl}^o N_k [\dot{v}_i] \quad (9)$$

Denoting  $Q_{ji}^o = N_i E_{ijkl}^o N_k$  as the elastic acoustic tensor, then the jump in the acceleration field is governed by the wave propagation equation accorded to Christoffel:

$$\boxed{(Q_{ji}^o - \rho c^2 \delta_{ji}) [\dot{v}_i] = 0} \quad (10)$$

where the wave propagation velocity  $c$  is determined by the eigenvalues ( $\rho c^2$ ) of the acoustic tensor and the jump of the acceleration by its eigenvector. Consequently, the positive definite acoustic tensor of linear elasticity results in positive wave speeds.

If during the load history the material becomes plastic, stress-induced anisotropy reduces the tangential stiffness properties and the propagation speed of acceleration waves will change accordingly. Thereby, a zero value of the lowest wave speed indicates a standing wave associated with formation of a discontinuity, and a complex eigenvalue ( $\rho c^2$ ) indicates instability in the form of divergence (flutter) - see [4].

The flow theory of plasticity distinguishes plastic loading from elastic unloading according to the alignment of the elastic trial stress rate  $\dot{\boldsymbol{\sigma}}_e$  with the normal to the yield surface  $\mathbf{n}$ : thus plastic loading takes place when  $\mathbf{n} : \dot{\boldsymbol{\sigma}}_e = \mathbf{n} : \mathbf{E}_o : \dot{\boldsymbol{\epsilon}} > 0$ . In that case, plastic consistency and the additive strain decomposition provide a plastic multiplier  $\dot{\lambda}$  that is strictly positive :

$$\dot{\lambda} = \frac{\langle \mathbf{n} : \dot{\boldsymbol{\sigma}}_e \rangle}{h_p} \quad \text{with the hardening parameter} \quad h_p = H_p + \mathbf{n} : \mathbf{E}_o : \mathbf{m} > 0 \quad (11)$$

where  $\mathbf{m}$  designates the flow direction of the plastic flow rule  $\dot{\boldsymbol{\epsilon}}_p = \dot{\lambda} \mathbf{m}$ . In the domain, where  $\boldsymbol{\sigma} \in C^0$ , its derivatives exist but they are not necessarily continuous. Thus the tangent stiffness tensor depends on the loading condition:

$$\dot{\boldsymbol{\sigma}} = \mathbf{E}_t : \dot{\boldsymbol{\epsilon}} \quad \text{where} \quad \mathbf{E}_t = \begin{cases} \mathbf{E}_o - \frac{1}{h_p} \mathbf{E}_o : \mathbf{m} \otimes \mathbf{n} : \mathbf{E}_o & \text{if } \mathbf{n} : \dot{\boldsymbol{\sigma}}_e > 0 \\ \mathbf{E}_o & \text{if } \mathbf{n} : \dot{\boldsymbol{\sigma}}_e \leq 0 \end{cases} \quad (12)$$

Consequently, the jump of the stress rate across the discontinuity surface  $\mathcal{S}$  reads:

$$[\dot{\boldsymbol{\sigma}}] = \mathbf{E}_o : [\dot{\boldsymbol{\epsilon}}] - \frac{1}{h_p} \mathbf{E}_o : \mathbf{m} [\langle \mathbf{n} : \dot{\boldsymbol{\sigma}}_e \rangle] \quad (13)$$

If we define  $\xi$  as in [6]:  $[\langle \mathbf{n} : \dot{\boldsymbol{\sigma}}_e \rangle] = \xi [\mathbf{n} : \dot{\boldsymbol{\sigma}}_e]$ , the wave type depends on the value of this parameter:

1. **Plastic Wave:** if  $(\langle \mathbf{n} : \dot{\sigma}_e \rangle)^+ > 0$  and  $(\langle \mathbf{n} : \dot{\sigma}_e \rangle)^- > 0$ , then  $\xi = 1$  ;
2. **Elastic - Plastic Wave:** if  $(\langle \mathbf{n} : \dot{\sigma}_e \rangle)^+ > 0$  and  $(\langle \mathbf{n} : \dot{\sigma}_e \rangle)^- \leq 0$  defines an unloading wave, and  $(\langle \mathbf{n} : \dot{\sigma}_e \rangle)^+ \leq 0$  and  $(\langle \mathbf{n} : \dot{\sigma}_e \rangle)^- > 0$  a reloading wave, then  $\xi \in (0, 1)$  ;
3. **Elastic Wave:** if  $(\langle \mathbf{n} : \dot{\sigma}_e \rangle)^+ < 0$  and  $(\langle \mathbf{n} : \dot{\sigma}_e \rangle)^- < 0$ , then  $\xi = 0$ .

The relationship between the stress and the strain increment jump becomes:

$$[\dot{\sigma}] = E_o : [\dot{\epsilon}] - \frac{\xi}{h_p} E_o : \mathbf{m} [\langle \mathbf{n} : \dot{\sigma}_e \rangle] = \left( E_o - \frac{\xi}{h_p} E_o : \mathbf{m} \otimes \mathbf{n} : E_o \right) : [\dot{\epsilon}]$$

$$[\dot{\sigma}] = E_i^* : [\dot{\epsilon}] \quad \text{with} \quad E_i^* = E_o - \frac{\xi}{h_p} E_o : \mathbf{m} \otimes \mathbf{n} : E_o \quad (14)$$

Following the derivation of (9), taking into account symmetries in the stress and strain tensor, the elastic-plastic acoustic tensor reads:

$$Q_{ji}^t = N_i E_{ijpq}^t N_k = Q_{jt}^o - \frac{\xi}{h_p} a_j b_i \quad (15)$$

where  $a_j = N_i E_{ijpq}^o m_{pq}$  and  $b_l = n_{rs} E_{rskl}^o N_k$ .

Consider the eigenbasis formed by the eigenvectors of the elastic acoustic tensor. If  $\eta_3^o \leq \eta_2^o \leq \eta_1^o$  denote the eigenvalues, then  $Q_o$  has the format:

$$Q_o = \begin{pmatrix} \eta_1^o & 0 & 0 \\ 0 & \eta_2^o & 0 \\ 0 & 0 & \eta_3^o \end{pmatrix} \quad (16)$$

Using (15) the elastoplastic acoustic tensor writes:

$$Q_t = \begin{pmatrix} \eta_1^o - \frac{\xi}{h_p} a_1 b_1 & -\frac{\xi}{h_p} a_1 b_2 & -\frac{\xi}{h_p} a_1 b_3 \\ -\frac{\xi}{h_p} a_2 b_1 & \eta_2^o - \frac{\xi}{h_p} a_2 b_2 & -\frac{\xi}{h_p} a_2 b_3 \\ -\frac{\xi}{h_p} a_3 b_1 & -\frac{\xi}{h_p} a_3 b_2 & \eta_3^o - \frac{\xi}{h_p} a_3 b_3 \end{pmatrix} \quad (17)$$

Its eigenvalues  $\eta$  are the roots of the characteristic polynomial:

$$f(\eta) = \begin{vmatrix} (\eta_1^o - \eta) - \frac{\xi}{h_p} a_1 b_1 & -\frac{\xi}{h_p} a_1 b_2 & -\frac{\xi}{h_p} a_1 b_3 \\ -\frac{\xi}{h_p} a_2 b_1 & (\eta_2^o - \eta) - \frac{\xi}{h_p} a_2 b_2 & -\frac{\xi}{h_p} a_2 b_3 \\ -\frac{\xi}{h_p} a_3 b_1 & -\frac{\xi}{h_p} a_3 b_2 & (\eta_3^o - \eta) - \frac{\xi}{h_p} a_3 b_3 \end{vmatrix}$$

$$= (\eta_1^o - \eta) (\eta_2^o - \eta) (\eta_3^o - \eta) - \frac{\xi}{h_p} [a_1 b_1 (\eta_2^o - \eta) (\eta_3^o - \eta) + a_2 b_2 (\eta_1^o - \eta) (\eta_3^o - \eta) + a_3 b_3 (\eta_1^o - \eta) (\eta_2^o - \eta)] \quad (18)$$

The roots of the characteristic polynomial may be found analytically or numerically if the material characteristics,  $\mathbf{n}$  and  $\mathbf{m}$ , and the wave type  $\xi$  are defined. From the eigenvalues the corresponding eigenvectors and thus the directions of the acceleration jumps may be obtained, but not their magnitudes. If all roots are positive, then the wave propagation velocities  $c_i = \sqrt{\eta_i/\rho}$  are also positive, whereby the corresponding eigenvectors define their polarization directions. A zero value represents a standing wave in a non-propagating medium, while negative roots indicate instability to small disturbances defining a pair of complex wave speeds that correspond to a "flutter instability" [4]. In that case, only one wave speed remains real, while there are two complex-conjugate ones.

### Localization Condition of Weak Discontinuities

In contrast to the standing wave argument, localization analysis detects the formation of spatial discontinuities in the kinematic fields across singularity surfaces that might emerge in an overly stressed body. The formation of a weak discontinuity assumes that a second order singularity appears, where the displacement and velocity fields are still continuous:

$$[\mathbf{u}] = \mathbf{u}^+ - \mathbf{u}^- = 0, \quad [\dot{\mathbf{u}}] = \dot{\mathbf{u}}^+ - \dot{\mathbf{u}}^- = 0$$

while the velocity gradients exhibit jump conditions,

$$[\nabla_x \dot{\mathbf{u}}] = \nabla_x \dot{\mathbf{u}}^+ - \nabla_x \dot{\mathbf{u}}^- \neq 0, \quad [v_{i,j}] = v_{i,j}^+ - v_{i,j}^- \neq 0_{ij} \quad (19)$$

For the sake of argument we state the formulation in direct and indicial notation. Applying Maxwell's Compatibility Condition [7], the jump condition of the velocity gradient must be a rank-one tensor:

$$[\nabla_x \dot{\mathbf{u}}] = \dot{\gamma} \mathbf{M} \otimes \mathbf{N}, \quad [v_{i,j}] = \dot{\gamma} M_i N_j \quad (20)$$

As before,  $\mathbf{N}$  defines the normal of the discontinuity surface ( $\mathcal{S}$ ) and  $\mathbf{M}$  designates the jump direction, and  $\dot{\gamma}$  the jump amplitude. Comparing with the Hadamard compatibility condition in 4, we recognize the physical meaning of the jump amplitude and the polarization direction, i.e.

$$\dot{\gamma} M_i = -[\dot{v}_i]/c, \quad \dot{\gamma} = -|\dot{v}_i|/c \quad (21)$$

Introducing the strain-displacement relations of classical continua, the jump in the strain rate is

$$[\dot{\boldsymbol{\epsilon}}] = \frac{1}{2} [\nabla_x^t \dot{\mathbf{u}} + \nabla_x \dot{\mathbf{u}}] = \frac{\dot{\gamma}}{2} (\mathbf{N} \otimes \mathbf{M} + \mathbf{M} \otimes \mathbf{N}) = \dot{\gamma} (\mathbf{N} \otimes \mathbf{M})^{sym} \quad (22)$$

**Remark:** The symmetrizing condition of the strain rate expression transforms the rank-one tensor of the velocity gradient (20) into a rank-two tensor (22), except when  $\mathbf{M} \parallel \mathbf{N}$  indicating a mode I discontinuity of cracking. In other terms, the partial derivatives tangential to the discontinuity surface remain continuous, while the partial derivatives perpendicular to the singularity surface exhibit jumps.

Assuming that the onset of localization takes place when both sides of the singularity surface are in a state of plastic loading, then the tangential elastoplastic constitutive law together with the strain rate jump, and taking into consideration the minor symmetries of the tangent material operator, lead to the jump of stress rate:

$$[\dot{\boldsymbol{\sigma}}] = [\mathbf{E}_t^* : \dot{\boldsymbol{\epsilon}}] = \mathbf{E}_t : [\dot{\boldsymbol{\epsilon}}] = \dot{\gamma} \mathbf{E}_t : (\mathbf{N} \otimes \mathbf{M})^{sym} \quad (23)$$

According to Cauchy's lemma, the traction rate vector  $\dot{\mathbf{t}}$  has to remain continuous across any surface in the interior of a solid (see figure 1). Thus, we may combine this requirement with the constitutive and kinematic equations, the localization condition as long as the two faces along the singularity surface remain in full contact:

$$[\dot{\mathbf{t}}] = \mathbf{N} \cdot [\dot{\boldsymbol{\sigma}}] = (\mathbf{N} \cdot \mathbf{E}_t \cdot \mathbf{N}) \cdot (\dot{\gamma} \mathbf{M}) = \mathbf{Q}_t \cdot (\dot{\gamma} \mathbf{M}) = 0 \quad (24)$$

In spite of the traction continuity requirement the stress tensor still exhibits discontinuities. In fact, complementary to the jump condition of strain rates, the normal stress components tangential to the discontinuity surface exhibit now jump conditions, while the normal stress component normal to the surface and the shear stress component remain continuous. In analogy to the acoustic tensor 15,  $\mathbf{Q}_t = \mathbf{N} \cdot \mathbf{E}_t \cdot \mathbf{N}$  defines the tangential localization tensor in elastoplastic continua, whereby the eigenvector  $\mathbf{M}$  indicates the direction of the velocity jump. Thus discontinuous bifurcation initiates when the localization tensor exhibits a singularity, i.e. when

$$\boxed{\det(\mathbf{Q}_t) = 0} \quad (25)$$

In analogy to the stationarity condition of acceleration waves, the localization condition characterizes the formation of weak discontinuities in terms of the bifurcation argument above. Recall, a weak discontinuity of second order in the displacement field signals the onset of localized failure, that precedes formation of strong discontinuities of first order in the displacement field.

**Remark:** The localization condition (25) implies that at the onset of localization both sides of the singularity surface are in a state of loading,  $[\mathbf{E}_t] = \mathbf{0}$ , and that the traction rate vector  $\dot{\mathbf{t}}$  is continuous across the singularity surface (figure 1, right),  $[\dot{\mathbf{t}}] = \mathbf{N} \cdot [\dot{\boldsymbol{\sigma}}] = \mathbf{0}$ . In analogy to fracture mechanics, the eigenvector  $\mathbf{M}$  of  $\det(\mathbf{Q}_t) = 0$  characterizes the discontinuous failure mode, thus  $\mathbf{M} \parallel \mathbf{N}$  indicates mode I, and  $\mathbf{M} \perp \mathbf{N}$  indicates mode II failure.

### Geometrical Localization Analysis

In the case of localization, the important aspect is the direction  $\mathbf{N}$  of the normal to the discontinuity surface which is an implicit function of the localization tensor  $\mathbf{Q}_t = \mathbf{N} \cdot \mathbf{E}_t \cdot \mathbf{N}$ , where  $\det(\mathbf{Q}_t) = 0$ . For the sake of argument, let us consider the elastoplastic bifurcation process in a non-associated Drucker-Prager solid where the plastic yield condition and the plastic potential are linear functions of the first principal invariant and the second deviatoric invariant :

$$F(I_1, J_2) = \sqrt{J_2} + \alpha_1 I_1 - \beta_1 = 0 \quad \text{and} \quad Q(I_1, J_2) = \sqrt{J_2} + \alpha_2 I_1 - \beta_2 = 0 \quad (26)$$

$$\alpha_i = \frac{f'_c - f'_t}{\sqrt{3}(f'_c + f'_t)}; \quad \beta_i = \frac{2 f'_c f'_t}{\sqrt{3}(f'_c + f'_t)}$$

Here the two parameters  $\alpha_i, \beta_i$  in the yield function and the plastic potential are calibrated in terms of strength values in uniaxial tension and compression:  $f'_t$  and  $f'_c$ . The gradients of the yield function and the plastic potential with respect to stress are

$$\mathbf{n} = \frac{\partial F}{\partial \boldsymbol{\sigma}} = \frac{1}{2\sqrt{J_2}} \mathbf{s} + \alpha_1 I_1 \mathbf{I}_2 \quad \text{and} \quad \mathbf{m} = \frac{\partial Q}{\partial \boldsymbol{\sigma}} = \frac{1}{2\sqrt{J_2}} \mathbf{s} + \alpha_2 I_1 \mathbf{I}_2 \quad (27)$$

The elastoplastic tangent stiffness of the non-associated Drucker-Prager solid leads to the localization tensor in the form :

$$\mathbf{Q}_t = \mathbf{N} \cdot \mathbf{E}_t \cdot \mathbf{N} = \mathbf{Q}_o - \frac{1}{h_p} \mathbf{a} \otimes \mathbf{b} \quad (28)$$

where  $\mathbf{Q}_o = \mathbf{N} \cdot \mathbf{E}_o \cdot \mathbf{N}$ , and where  $\mathbf{a} = \mathbf{N} \cdot \mathbf{E}_o : \mathbf{m}$  and  $\mathbf{b} = \mathbf{n} : \mathbf{E}_o \cdot \mathbf{N}$  designate the so-called traction vectors. Using an intriguing eigenvalue property of rank-one modifications of the unit tensor, see [8] and [9], one is able to recast the localization condition of the generalized eigenvalue problem  $\mathbf{Q}_o^{-1} \cdot \mathbf{Q}_t = \mathbf{I}_2 - \frac{1}{h_p} \mathbf{Q}_o^{-1} \cdot \mathbf{a} \otimes \mathbf{b}$  and to convert the solution of  $\det(\mathbf{Q}_t) = 0$  into maximizing the hardening modulus  $H_p$  in the expression below :

$$H_p + \mathbf{n} : \mathbf{E}_o : \mathbf{m} = \mathbf{b} \cdot \mathbf{Q}_o^{-1} \cdot \mathbf{a} \quad (29)$$

Localization initiates when the hardening modulus  $H_p$  reaches a maximum for all possible orientations  $\mathbf{N} = \mathbf{N}(\theta)$ , or in other terms when the hardening modulus reaches a critical value for localization,  $H_{\sigma} = \max(H_p)$ .

This maximizing problem has been solved analytically using Lagrange's multipliers for stress-based isotropic non-associated elastoplasticity in [4]. Here we pursue a geometric solution of this problem that follows the original concept of the Mohr envelope in strength of materials, see [10] and [11]. In this approach, the critical localization directions and the maximum hardening modulus are determined with the aid of the geometric representation of stress in Mohr coordinates.

The normal and the resultant shear stress components ( $\sigma_N$  and  $\tau_N$ ) of the stress tensor  $\boldsymbol{\sigma}$  and the deviatoric stress  $\mathbf{s}$  on a plane with the normal  $\mathbf{N}$  are:

$$\sigma_N = \mathbf{N} \cdot \boldsymbol{\sigma} \cdot \mathbf{N}, \quad \tau_N = \mathbf{N} \cdot \mathbf{s} \cdot \mathbf{N}$$

$$\begin{aligned}\tau_N^2 &= (\mathbf{N} \cdot \mathbf{s}) \cdot (\mathbf{N} \cdot \mathbf{s}) - (\mathbf{N} \cdot \mathbf{s} \cdot \mathbf{N})^2 \\ \bar{\sigma}_N &= \frac{\sigma}{\sqrt{J_2}}, \quad \bar{s}_N = \frac{s}{\sqrt{J_2}}, \quad \bar{\tau}_N = \frac{\tau}{\sqrt{J_2}}\end{aligned}\quad (30)$$

The two terms of the analytic localization condition (29) reduce for the non-associated Drucker-Prager material to :

$$H_p + \mathbf{n} : \mathbf{E}_o : \mathbf{m} = H_p + E \left[ \frac{3 \alpha_1 \alpha_2}{1 - 2\nu} + \frac{1}{2(1 + \nu)} \right] \quad (31)$$

$$\begin{aligned}\mathbf{b} \cdot \mathbf{Q}_o^{-1} \cdot \mathbf{a} &= \frac{E}{2(1 + \nu)} \bar{\tau}_N^2 + E \frac{(1 + \nu)(1 - 2\nu)}{1 - \nu} \left[ \frac{1}{4(1 + \nu)^2} \bar{s}_N^2 \right. \\ &\quad \left. + \frac{\alpha_1 + \alpha_2}{2(1 + \nu)(1 - 2\nu)} \bar{s}_N + \frac{\alpha_1 \alpha_2}{(1 - 2\nu)^2} \right]\end{aligned}\quad (32)$$

Consequently, the localization condition traces the shape of an ellipse in the transformed Mohr coordinates of normal and shear stress :

$$\boxed{\frac{(\bar{\sigma}_N - \bar{\sigma}_o)^2}{A^2} + \frac{\bar{\tau}_N^2}{B^2} = 1} \quad (33)$$

where the center and the half-axes of the localization ellipse are defined by

$$\begin{aligned}\bar{\sigma}_o &= \frac{1}{3} \bar{I}_1 - \frac{1 + \nu}{1 - 2\nu} (\alpha_1 + \alpha_2) \\ B^2 &= \frac{2(1 + \nu)}{E} H_p + 1 + \alpha_1 \alpha_2 \frac{6(1 + \nu)}{1 - 2\nu} + (\alpha_1 - \alpha_2)^2 \frac{(1 + \nu)^2}{2(1 - \nu)(1 - 2\nu)} \\ A^2 &= \frac{2(1 - \nu)}{1 - 2\nu} B^2\end{aligned}\quad (34)$$

Contrary to the conical envelope of the Drucker-Prager yield condition, the localization envelope of the elastoplastic material formulation forms an ellipse in the transformed Mohr space, the center of which depends on the hydrostatic state of stress as well as the elastic and plastic material properties. Tangency between the elliptic localization envelope and the principal *Mohr Circle* of stress with the radius  $\bar{r} = 0.5(\sigma_1 - \sigma_3)/\sqrt{J_2}$  and the center  $\bar{\sigma}_c = 0.5(\sigma_1 + \sigma_3)/\sqrt{J_2}$

$$\boxed{(\bar{\sigma}_N - \bar{\sigma}_c)^2 + \bar{\tau}_N^2 = \bar{r}^2} \quad (35)$$

yields the critical hardening modulus  $H_{\sigma}$  illustrated in figure 2 when  $\bar{r} \leq A$ ,  $\bar{r} \leq B$ , and  $|\bar{\sigma}_c - \bar{\sigma}_o| \leq A - \bar{r}$  :

$$\begin{aligned}H_{\sigma} &= \frac{E}{2(1 + \nu)} \left\{ \frac{r^2}{J_2} + (1 - 2\nu) \left[ \frac{\sigma_c}{\sqrt{J_2}} - \frac{I_1}{3\sqrt{J_2}} + \frac{1 + \nu}{1 - 2\nu} (\alpha_1 + \alpha_2) \right]^2 \right. \\ &\quad \left. - 1 - \alpha_1 \alpha_2 \frac{6(1 + \nu)}{1 - 2\nu} - (\alpha_1 - \alpha_2)^2 \frac{(1 + \nu)^2}{2(1 - \nu)(1 - 2\nu)} \right\}\end{aligned}\quad (36)$$

with the critical localization angle  $\theta_{\sigma}$  :

$$\boxed{\tan^2 \theta_{\sigma} = \frac{r - \left[ \left( \sigma_c - \frac{1}{3} I_1 \right) (1 - 2\nu) + \sqrt{J_2} (\alpha_1 + \alpha_2) (1 + \nu) \right]}{r + \left[ \left( \sigma_c - \frac{1}{3} I_1 \right) (1 - 2\nu) + \sqrt{J_2} (\alpha_1 + \alpha_2) (1 + \nu) \right]}} \quad (37)$$

The analytical expressions of the critical hardening modulus and the localization directions developed

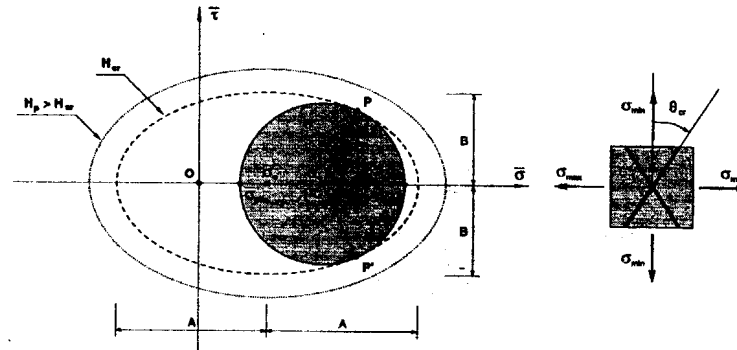


Figure 2: *Elliptic Localization Envelope and the Major Principal Mohr Circle of Stress.*

Table 1: *Yield Stresses, Critical Hardening Modulus and Failure Angles of Drucker-Prager Formulation in Three Dimensions ( $f'_c/f'_t = 2/1$ ).*

Loading Case	Stress Components			Failure Angle ( $\theta_{cr}$ )			$H_{cr}/E$
	$\sigma_1$	$\sigma_2$	$\sigma_3$	$\nu = 0.0$	$\nu = 0.2$	$\nu = 0.5$	
Compression	0.00	0.00	-2.00	41.81°	35.26°	24.09°	-0.2315
Shear	0.77	0.00	-0.77	33.68°	31.24°	27.37°	-0.0370
Tension	1.00	0.00	0.00	19.47°	21.42°	24.09°	-0.0093

in [11] indicate that the hardening modulus does not affect the critical localization angle.  $H_p$  changes only the size of the elliptic localization envelope, but not the center and not the half axes ( $A/B$ ) in equation (34). However, Poisson's ratio does change the shape and position of the ellipse, and it certainly affects the localization angle. Table 1 summarizes the stress components at yield, the predicted localization directions and the critical hardening modulus when an associated Drucker-Prager solid with  $\alpha_1 = \alpha_2$  is considered. We observe that the critical failure angle varies with Poisson's ratio. The critical hardening modulus however does not depend on Poisson's ratio if the flow rule is associated. We also note that, the localization condition is reached in three dimensions only when softening takes place, or alternatively when the Drucker-Prager solid loses normality in the case of non-associated flow. Comparing the localized failure modes in figure 3, the localization angles of the non-associated case are bounded by the those of the associated Drucker-Prager and the von Mises formulation.

**Remarks:** For associated plastic flow the critical hardening parameter must be negative in three dimensions, while in two dimensional analysis the localization condition may be reached for perfect plasticity ( $H_{cr} = 0$ ), see [11]. The localization angle in three dimensions depends on Poisson's ratio, while in two dimensions this angle and thus the localized failure mode remains fixed and does not vary with the state of stress. In plane strain, due to the kinematic constraint, the stress state at the stationary point has to be considered, when  $\dot{\sigma} \rightarrow 0$ . At that point the principal stress values differ from the stress values at the initial yield point.

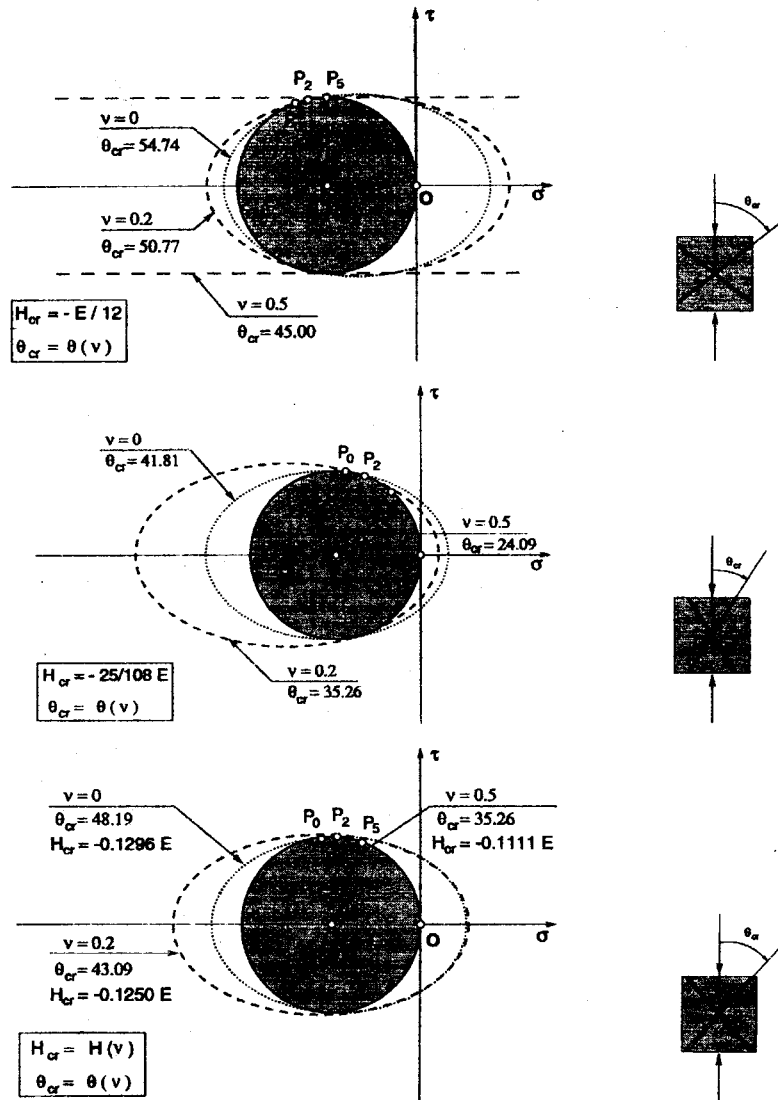


Figure 3: Localization Properties in Uniaxial Compression: von Mises (top), Associated Drucker-Prager (middle), and Non-Associated Drucker-Prager (bottom).

### Uniaxial Compression Problem

For illustration of the analytical and geometrical localization results, we examine the load-deformation of an elastoplastic solid in uniaxial compression in order to assess the localization properties of von Mises versus associated and non-associated Drucker-Prager softening behavior. The material properties are in this example:

$$E = 2000.0 \text{ ksi}; \nu = 0.2; f'_c = 2.0 \text{ ksi}$$

$$f'_t = \begin{cases} 2.0 \text{ ksi} & \text{Mises} \\ 1.0 \text{ ksi} & \text{Drucker-Prager} \end{cases} \quad (38)$$

whereby softening is described in terms of a cubic parabola with zero slope at the peak and the residual stress levels. Figure 4 illustrates the response behavior in terms of axial and lateral stress-strain components (left). Note that the non-associated Drucker-Prager formulation exhibits for uniaxial compression the same axial and lateral deformation characteristics as the von Mises formulation does because an incompressible flow potential of the von Mises type is used. The figure on the right depicts the hardening or rather the softening moduli at different loading stages. It illustrates that the softening von Mises formulation reaches the critical hardening modulus of localization right after peak, while the associated Drucker-Prager formulation never reaches the critical value. The figure also shows the destabilizing effect of the non-associated Drucker-Prager model which almost reaches localization when the plastic hardening modulus  $H_p^{na} = \min$ . Finally, we observe that the critical hardening modulus to initiate localization remains constant during proportional loading, and that the corresponding localization directions also remain fixed. This observation indicates that the localized failure mode does not depend on the level of stress and remains fixed during proportional loading.

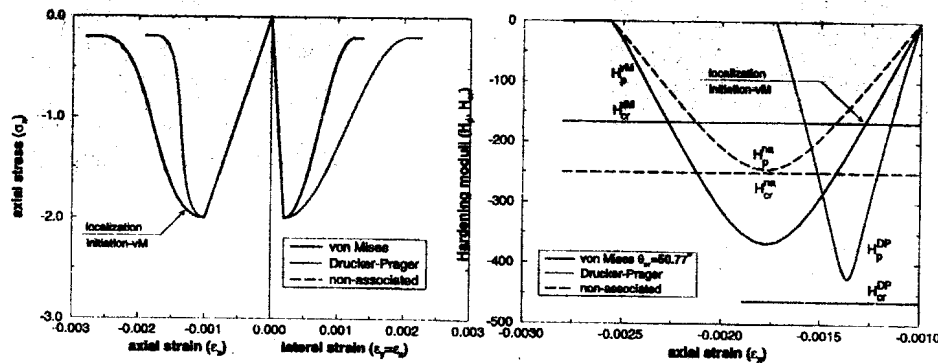


Figure 4: *Softening Response Behavior in Uniaxial Compression (left), Localization Analysis of Critical Hardening Moduli (right) of von Mises, Drucker-Prager and Non-Associated Drucker-Prager Materials.*

### DISCONTINUOUS FAILURE AT THE STRUCTURAL LEVEL

Localization analysis of discontinuous bifurcation and is an important first step to understand and model brittle and ductile failure in materials. The failure angle can be determined analytically and it was shown that the corresponding failure mode does not change during proportional loading. This observation helps to design a finite element mesh layout that is able to capture localized failure. According to the studies in [12], the mesh layout should be aligned with the eventual localization direction to capture the localized failure mode without undue mesh bias.

The following study shows that the analytical localization angles coincide with the failure directions obtained from finite elements analysis at the structural level. In fact, the same structural

failure modes are obtained using random meshes as well as regular meshes, only the ductility changes significantly with initial imperfections. Consequently, a study of a two-phase particle composite is carried out to introduce imperfections in a natural manner. The computational results in [11] show that the failure mode in the composite is similar to the failure mode of the homogeneous matrix material, as long as random distributions of particles are considered at volume fractions representative for dispersed media.

#### Failure Analysis of a Two-Phase Particle Composite

The test specimen is a square domain that is subjected to compressive loading (see figure 5-left). The random mesh layout of the representative "unit-square" is illustrated in figure 5-right which shows the geometry and boundary conditions. The compression test is performed in displacement control, imposing uniform vertical displacements  $u$  at the upper surface nodes. Voronoi-polygonization is

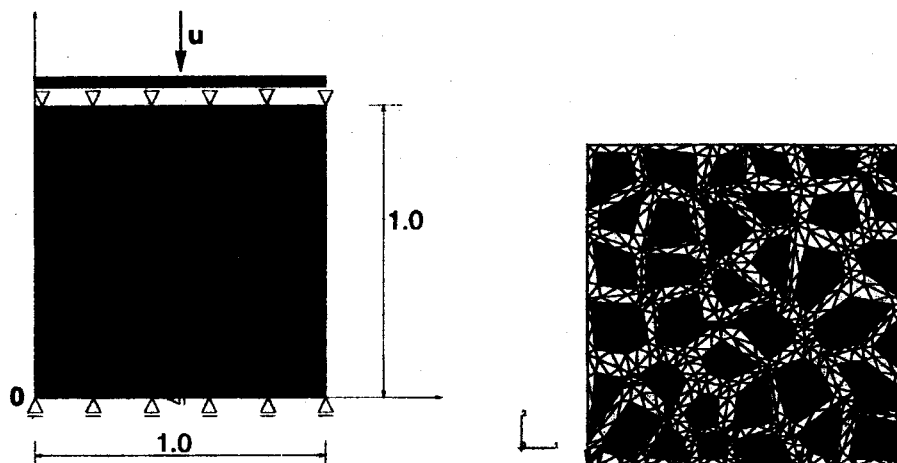


Figure 5: *Square Compression Specimen (left) and Finite Element Discretization (right) using a Random Mesh to generate a Two-Phase Composite Based on Voronoi Polygonization of  $6 \times 6 = 36$  aggregates,  $A_a/A_m = 0.6 = \text{const.}$*

performed using a  $6 \times 6$  mesh of elastic particles as described by Stankowski in [13]. The resulting mesh, with 1656 constant strain triangles in the elastoplastic matrix and the elastic particles is being analysed with the finite element code ABAQUS [14]. In an attempt to relate to the properties of normal strength concrete, the elastic properties of the aggregate particles are assumed to be considerably higher than those of the elastoplastic cementitious matrix material:

$$\begin{aligned} E_m &= 2000. \text{ ksi} & \nu_m &= 0.2 \\ E_a &= 10000. \text{ ksi} & \nu_a &= 0.1 \end{aligned} \quad (39)$$

The yield strength of the Drucker-Prager matrix material is calibrated in terms of  $f'_c = 2.0 \text{ ksi}$ ,  $f'_t = 1.0 \text{ ksi}$ , whereby the compressive strength is modified according to isotropic softening varying the compressive strength with the equivalent plastic strain:

$$f'_c = \begin{cases} 2.0 \text{ ksi} & \bar{\epsilon}_p = 0 \\ 0.2 \text{ ksi} & \bar{\epsilon}_p = \bar{\epsilon}_p^{\text{max}} \end{cases} \quad (40)$$

A second order parabola describes the softening branch for  $\bar{\epsilon}_p \in [0, \bar{\epsilon}_p^{max} = 0.5]$ , where the maximum plastic strain for the residual stress is  $\bar{\epsilon}_p^{max} = 0.5$ . For the uniform specimen made of the Drucker-Prager matrix material, the analytical failure angle is obtained by both finite element analyses, using random as well as regular mesh layouts. In both cases, the localized deformations concentrate in one element layer, however, for the random mesh, the formation of the localization band is delayed due to misalignment of the mesh with the failure direction.

The progressive failure study in the two-phase particle composite is carried out in order to identify whether the failure directions remain close to the ones predicted by the homogeneous material. In the composite study there is no need for a weak element, as failure is triggered by the multiple stress concentrators in the aggregate-matrix interfaces. The main results of the composite failure study with 36 aggregates are shown in figure 6. It depicts the deformed shape, contour plots of the plastic strains, and a comparison between the aggregate, matrix and the composite responses. The stiffness and strength properties of the composite specimen are higher than the ones of the uniform elastoplastic matrix material, but in return, the composite is a lot more fragile, when compared with the matrix alone. The increased brittleness of the composite specimen is due to the mismatch in mechanical properties of the two constituents and the stress concentrations in the particle interfaces. Clearly, matrix failure initiates at the aggregate-matrix interface, and it propagates in the matrix in the direction close to the localization direction of the uniform matrix material. The localization process is accelerated due to multiple stress concentrators at the aggregate-matrix interface. Consequently, the softening branch is much steeper (see top figure). The stiffness of the composite is higher than the matrix stiffness, and its strength is increased by almost 40%.

As for von Mises material in plane strain, the aggregate particles induces lateral confinement in the matrix and, as a result, the matrix does behave similar to the uniaxial strain case where the stresses increase without bounds, see figure 7. However, in some locations triaxial tension develops, the stress path slides down the Drucker-Prager cone close to the vertex point, where the numerical analysis terminates prematurely. The important observation of the composite study in plane strain is, that distinct failure bands do not form whatsoever, and that a diffuse deformation process does emerge in which the plastic deformations are distributed evenly throughout the specimen.

### CONCLUDING REMARKS

The paper did outline the kinematical concepts behind discontinuities in cohesive-frictional materials. Our focus was localization analysis at the material level. A geometrical solution of the localization condition was developed for non-associated and pressure-sensitive plasticity in order to detect the onset and the orientation of discontinuous failure modes in terms of a Mohr-type envelope approach. This geometrical concept connects modern localization analysis and the traditional strength concept of the Mohr envelope condition, and it provides new insight into the proximity of the stress state to discontinuous failure.

The failure predictions of Drucker-Prager materials were studied also at the structural level for comparison with localization results at the constitutive level. After highly stressed regions reach the localization condition, mesh objectivity with regard to ductility is lost in general, and the slope of structural softening depends greatly on the element size and on the element orientation. Local instabilities of the global equilibrium configuration are activated, and failure bands begin to propagate throughout the structure. Thereby, the orientation of these failure bands follows closely the analytical localization predictions at the constitutive level.

For illustration of the effect of initial imperfections, a two-phase particle composite was analysed. Plane stress analysis of the elastoplastic Drucker-Prager matrix did result in the same localized failure mode in the composite specimen as the uniform Drucker-Prager specimen did. In contrast, plane strain analysis did result in diffuse failure throughout the matrix of the composite specimen because confinement of the out-of-plane kinematic constraint did prevent formation of localized failure.

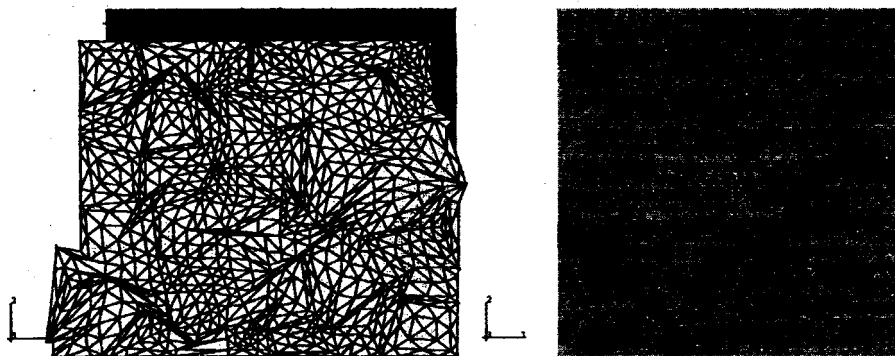
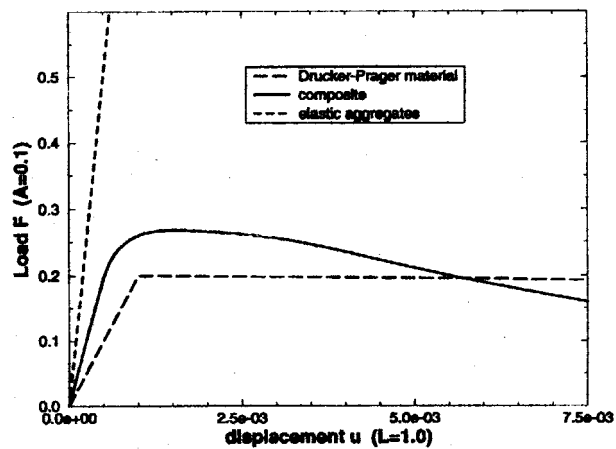


Figure 6: *Progressive Failure in Two-Phase Composite with Drucker-Prager Matrix - Compression Test in Plane Stress.*

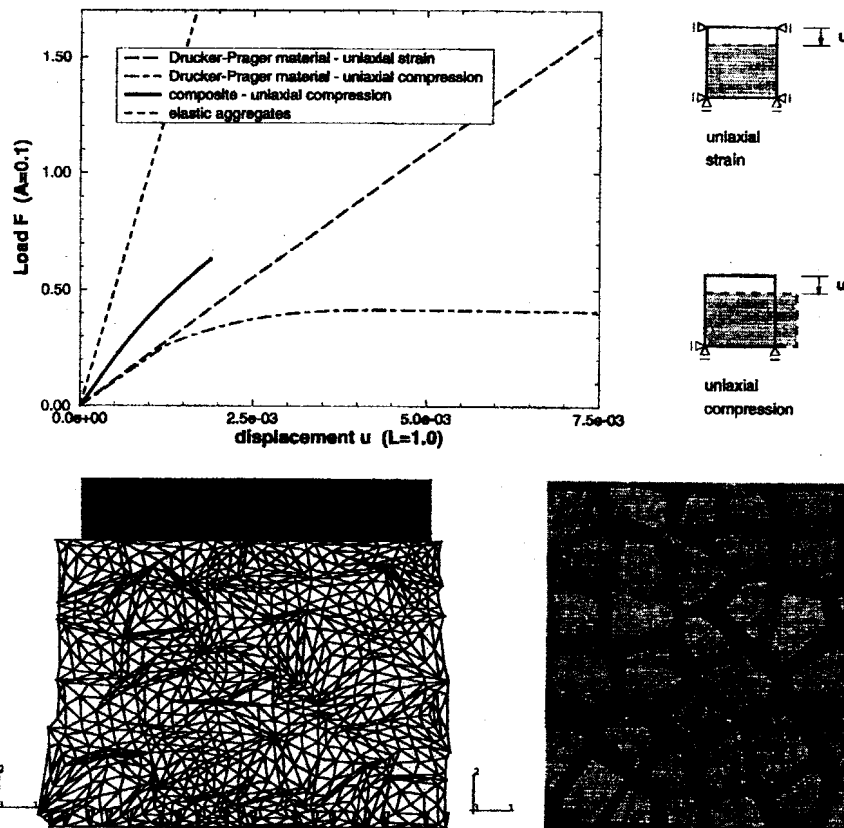


Figure 7: Progressive Failure in Two-Phase Composite with Drucker-Prager Matrix - Compression Test in Plane Strain.

### Acknowledgments

The authors wish to thank the US-AFOSR and Dr. J. Chang and Dr. B. Sanders for the financial support under grant 49620-96-1-0112 to the University of Colorado, Boulder.

### References

- [1] ETSE, G. AND WILLAM, K., [1994], "A Fracture Energy-Based Constitutive Formulation for Inelastic Behavior of Plain Concrete," *ASCE-J. Engrg. Mechcs*, Vol. 120, pp. 1983-2011.
- [2] WILLAM, K. AND IORDACHE, M.-M., [1994], "Fundamental Aspects of Failure Modes in Brittle Solids", in *Fracture and Damage in Quasibrittle Materials*, Z. Bažant, Z. Bittnar, J. Jirašek and J. Mazars Eds., E&F Spon, Chapman and Hall, London, pp. 35-67.
- [3] HILL, R., [1962], "Acceleration waves in solids", *J. Mech. Phys. Solids*, Vol. 10, pp. 1-16.
- [4] RUDNICKI, J.W. AND RICE, J.R., [1975], "Conditions for the Localization of Deformations in Pressure-Sensitive Dilatant Materials", *J. Mech. Phys. Solids*, Vol. 23, pp. 371-394.
- [5] HADAMARD, J., [1901], "*Sur la propagation des ondes*", *Bull. Soc. Math. France*, Vol. 29, pp. 50-60.
- [6] LUBLINER, J., [1990], "*Plasticity Theory*", Macmillan Publishing Co., NY, Collier Macmillan Publishers, London, UK.
- [7] MAXWELL, J.C., [1873], "*A Treatise in Electricity and Magnetism*", Oxford, UK.
- [8] OTTOSEN, N.S. AND RUNESSON, K., [1991], "Properties of Discontinuous Bifurcation Solutions in Elastoplasticity", *Int. J. Solids Structures*, Vol. 27, No. 4, pp. 401-421.
- [9] RIZZI, E., MAIER, G. AND WILLAM, K., [1996], "On Failure Indicators in Multi-Dissipative Materials", *Int. J. Solids Structures*, Vol. 33, No. 20-22, pp. 3187-3214.
- [10] BENALLAL, A. AND COMI, C., [1996], "Localization Analysis via a Geometrical Method", *Int. J. Solids and Structures*, Vol. 33, No. 1, pp. 99-119.
- [11] IORDACHE, M.-M., [1996], "*Failure Analysis of Classical and Micropolar Elastoplastic Materials*", Ph.D. Dissertation, CEAE-Department, University of Colorado at Boulder, Boulder, CO, USA.
- [12] STEINMANN, P. AND WILLAM, K., [1994], "Finite-Element Analysis of Elastoplastic Discontinuities", *ASCE-J. Engrg. Mechcs*, Vol. 120, pp. 2428-2442.
- [13] STANKOWSKI, T., [1990], "*Numerical Simulation of Progressive Failure in Particle Composites*", Ph.D. Dissertation, CEAE-Department, University of Colorado at Boulder, Boulder, CO, USA.
- [14] HIBBIT, KARLSSON & SORENSEN, [1995], *ABAQUS- User's Manual, Version 5.5*, HKS Inc. Pawtucket, RI, USA.